Journal of Nuclear Materials 468 (2016) 232–239

Contents lists available at ScienceDirect

Journal of Nuclear Materials

journal homepage: www.elsevier.com/locate/jnucmat

Characterization and comparative analysis of the tensile properties of five tempered martensitic steels and an oxide dispersion strengthened ferritic alloy irradiated at ≈295 °C to ≈6.5 dpa

S.A. Maloy [a, *], T.A. Saleh [b], O. Anderoglu [a], T.J. Romero [c], G.R. Odette [d], T. Yamamoto [d], S. Li [d], J.I. Cole [e], R. Fielding [f]

[a] MST-8, Los Alamos National Laboratory, Los Alamos, NM 87545, USA
[b] MST-16, Los Alamos National Laboratory, Los Alamos, NM 87545, USA
[c] C-IIAC, Los Alamos National Laboratory, Los Alamos, NM 87545, USA
[d] Department of Mechanical Engineering, University of California Santa Barbara, Santa Barbara, CA 93106-5070, USA
[e] Nuclear Science User Facilities, Idaho National Laboratory, Idaho Falls, ID 83415, USA
[f] Fuel Fabrication and Characterization Department, Idaho National Laboratory, Idaho Falls, ID 83415, USA

HIGHLIGHTS

- Tensile tests were performed at 25 and 300 °C on 6 ferritic steels irradiated to 6.5 dpa at 295 °C in the Advanced Test Reactor.
- The irradiated true stress/true strain curves deform by strain softening, nearly perfectly plastic or strain hardening.
- The heat of 12Cr HT-9 steel has a much higher uniform elongation after irradiation than observed for earlier heats.
- This new heat of HT-9 has lower interstitial free nitrogen than previous heats.

ARTICLE INFO

Article history:
Received 7 May 2015
Received in revised form
14 July 2015
Accepted 24 July 2015
Available online 6 August 2015

Keywords:
Ferritic
Irradiation
Cladding
Reactor

ABSTRACT

Tensile test results at 25 and 300 °C on five 9-12Cr tempered martensitic steels and one 14Cr oxide dispersion strengthened alloy, that were side-by side irradiated to 6.5 dpa at 295 °C in the Advanced Test Reactor (ATR), are reported. The engineering stress–strain curves are analyzed to provide true stress –strain constitutive $\sigma(\varepsilon)$ laws for all of these alloys. In the irradiated condition, the $\sigma(\varepsilon)$ fall into categories of: strain softening, nearly perfectly plastic and strain hardening. Increases in yield stress ($\Delta\sigma_y$) and reductions in uniform strain ductility (e_u) are observed, where the latter can be understood in terms of the alloy's $\sigma(\varepsilon)$ behavior. Increases in the average $\sigma(\varepsilon)$ in the range of 0–10% strain are smaller than the corresponding $\Delta\sigma_y$, and vary more from alloy to alloy. The data are also analyzed to establish relations between $\Delta\sigma_y$ and coupled changes in the ultimate stresses as well as the effects of both test temperature and the unirradiated yield stress (σ_{yu}). The latter shows that higher σ_{yu} correlates with lower $\Delta\sigma_y$. In five out of six cases the effects of irradiation are generally consistent with previous observations on these alloys. However, the particular heat of the 12Cr HT-9 tempered martensitic steel in this study has a much higher e_u than observed for earlier heats. The reasons for this improved behavior are not understood and may be microstructural in origin. However, it is noted that the new heat of HT-9, which was procured under modern quality assurance standards, has lower interstitial nitrogen than previous heats. Notably lower interstitial solute contents correlate with improved ductility and homogenous deformation in broadly similar steels.

Published by Elsevier B.V.

1. Introduction and background

A key objective of the Fuel Cycle Research and Development Program is to qualify advanced, high burn-up (to 40%) fast spectrum reactor fuel and cladding systems that transmute minor

* Corresponding author.
E-mail address: maloy@lanl.gov (S.A. Maloy).

http://dx.doi.org/10.1016/j.jnucmat.2015.07.039
0022-3115/Published by Elsevier B.V.

actinides, thereby helping to close the nuclear fuel cycle [1]. The cladding pin must contain the fuel and fission products at an extremely high level of reliability. Thus the cladding alloy must be resistant to high dose irradiation damage, up to a maximum of 400 dpa, over prototypic fast reactor temperatures of 350–550 °C, while in contact with the liquid metal coolant. In particular, cladding alloys must resist various irradiation degradation phenomena, like void swelling at intermediate temperatures (400–500 °C) and reductions of ductility and fracture toughness, particularly at temperatures below 400 °C.

It is well established that so-called ferritic/martensitic alloys have much better resistance to void swelling than austenitic alloys. In the former case incubation doses for significant swelling in fast reactor neutron environments of up to ≈200 dpa have been observed and are projected to be higher in some cases [2–7]. Note that the swelling incubation dpa decreases in the presence of high quantities of helium, roughly linearly with an increasing He/dpa ratio [5,6,8,9]. However, compared to austenitic steels, the degradation of toughness and ductility[1] at irradiation temperatures below ≈400 °C may be as, or even more, severe especially in the presence of large quantities of helium [3–6,10,11]. There is a large body of literature on irradiation effects on the tensile properties for a broad alloy class that is referred to here as tempered martensitic steels (TMS) containing 8–12%Cr [3,5,6,10–13]. The corresponding databases span decades of research, a wide variety of applications (fission, fusion and accelerator-based technologies) and a range of alloys in the broad TMS class. More recently, an emerging database on the effects of irradiation on the tensile properties of so-called oxide dispersion strengthened (ODS) steels has been developing, including for ODS nanostructured ferritic alloy (NFA) variants [5,11,12].

However, in their raw form, tensile test engineering stress–-strain data [s(e) – see below] provide only part of the constitutive information needed for reactor design and in-service safety assessments. For example, designs may limit nominal component stresses to a fraction of the ultimate engineering tensile stress, s_{uts}, and a minimum uniform engineering strain ductility, e_u. However, more quantitative designs and detailed safety assessments, typically based on the finite element method (FEM) code analysis, require true effective stress-effective strain constitutive laws, $\sigma(\varepsilon)$.

There is a modest, but significant, body of published results on irradiation effects on Charpy V-notch transition temperature shifts and a much smaller database on fracture master curve toughness shifts, ΔT_o [3,5,6,10–14]. The irradiation-induced changes in the fracture and constitutive properties are highly inter-related. For example, at lower irradiation temperatures the ΔT_o are primarily caused by, and can be related to, irradiation hardening, typically characterized by the change in yield stress, $\Delta\sigma_y$ [5,6,10,14–16]. However, it has been shown that the change in the true flow stress between 0 and 10% plastic strain, $\Delta\sigma_{10}$, is a better measure of hardening to relate to toughness temperature shifts [17]. In the hardening dominated regime, $\Delta T_o \approx 0.7\Delta\sigma_{10}$, in units of °C and MPa [5,6,10,14–17]. Finally we note that for FEM studies, fracture toughness data must account for cracked body size and geometry effects in a way that is very sensitive to the alloy's constitutive law, $\sigma(\varepsilon)$ [14–16,18–20].

Here we focus on irradiation effects on $\sigma(\varepsilon)$ constitutive laws derived from simple tensile tests carried out on specimens irradiated side-by-side. In spite of the large body of irradiated tensile test results, there has been remarkably little corresponding analysis of this collective database. Studies include deriving $\sigma(\varepsilon)$ from measured s(e); assessing, understanding and modeling the effects of alloy type, composition and starting microstructure on $\sigma(\varepsilon)$; and evaluating the inter-relationship between various tensile properties in both the unirradiated and irradiated conditions. This study is aimed at addressing some of these unmet opportunities.

2. Tensile test engineering s(e) data and σ(ε) constitutive laws: objectives

Standard tensile tests directly provide data on engineering stress and strain, s(e), defined in the usual way: "s" given by load divided by the initial cross section area and "e" given by the change in gauge length divided by its original length. Tensile properties are usually simply characterized by the engineering yield stress $s_y \approx \sigma_y$, the ultimate stress (s_{uts}), the uniform elongation (e_u) at the onset of necking, as well as the total elongation (e_t) and reduction in area (RA) at specimen rupture. Note, the so-called ductility and post yield stress measures are not true material properties since they depend on the gauge section cross-section shape and dimensions. It is trivial to convert s(e) to $\sigma(\varepsilon)$ up to the point of necking.[2] However, due to typically very low e_u after irradiation, tensile test s(e) that undergo nearly immediate necking cannot directly provide post-yielding $\sigma(\varepsilon)$. Plastic strains increase rapidly to high values in the necked region undergoing large geometry changes, where continued deformation occurs under complex triaxial stress states.[3] However, as described below, s(e) curves can be used to derive $\sigma(\varepsilon)$ up to large ε by iterative FEM calculations.

Increasing irradiation hardening is also often[4] accompanied by a greater degree of internal mesoscale flow localization in high strain, deformation softened shear bands [21–23]. While flow localization plays a role in reductions in $d\sigma(\varepsilon_u)/d\varepsilon$, the irradiated e_u (or ε_u) is more generally controlled by the classical Considere's plastic instability criterion given by

$$d\sigma(\varepsilon)/d\varepsilon < \sigma(\varepsilon). \quad (1)$$

Thus increases in $\sigma(\varepsilon)$ and decreases in $d\sigma(\varepsilon)/d\varepsilon$ *combine* to reduce ε_u.

In this short paper we focus on the effects of irradiation to about ≈6.5 dpa at ≈295 °C, on the tensile properties of five 8-12Cr TMS's and one ODS alloy. These irradiation conditions result in large increases in the yield stress (σ_y) and flow stress [$\sigma(\varepsilon)$], $\Delta\sigma_y$ and $\Delta\sigma(\varepsilon)$, up to several hundred MPa. The strength increases coincide with large reductions in the e_{uu} to e_{ui}, and more modest reductions in the e_{tu} to e_{ti}, and corresponding post-necking total strains ($\varepsilon_{tu} - \varepsilon_{uu}$) to ($\varepsilon_{ti} - \varepsilon_{ui}$). Here the subscripts u and i designate the unirradiated and irradiated conditions, respectively. The irradiated tensile test rupture process remains ductile and occurs by microvoid nucleation, growth and coalescence. Thus the major structural degradation impact of these irradiation conditions is a severe reduction of plastic strain at the maximum load under tensile test conditions,[5] as characterized by the uniform elongation, e_{ui}.

Here we contrast and analyze the tensile properties of the 5 TMS and an ODS alloy that were irradiated side-by-side in the Nuclear Science Users Facility (NSUF) UCSB ATR-1 irradiation experiment.

[1] It is very important to note that fracture toughness and ductility are not the same properties, although they are often confused.

[2] For uniformly deforming gauge sections, $\sigma(\varepsilon) = s(e)(1 + e)$ and $\varepsilon = \ln(1 + e)$.

[3] The $\sigma(\varepsilon)$ derived from tensile tests are assumed to represent effective stress and strain, which can be used under multi-axial loading conditions. Modeling plastic deformation also requires a proper description of the governing flow potential (like J_2 flow theory) and associated flow-hardening rules.

[4] Flow localization does not always occur, especially under precipitation dominated hardening conditions. Localization is most often associated with hardening dominated by dislocation loops.

[5] Note low strain plastic instabilities are a characteristic of the tensile loading geometry and, for example, do not occur under bending or compression loading.

Four of the five normalized and tempered TMS alloys contain ≈8–9% Cr, while the other contains ≈12% Cr. The ODS alloy is a 14% Cr nearly fully ferritic stainless steel (MA957) that lies outside the Fe–Cr γ-loop. This fine grained ODS variant, also known as a NFA since it contains an ultrahigh density of nm-scale complex oxide precipitates, is characterized by high strength, substantial tensile ductility and remarkable resistance to irradiation damage [5,6,10,15,24,25].

The main objectives of this work include addressing the following:

To derive true stress–strain constitutive σ(ε) laws from the engineering stress strain s(e) curves; only the results of this analysis are shown here.

To determine how the hardening and ductility loss trends intercompare for the 9Cr TMS, the 12Cr TMS and the 14Cr ODS alloy in the side-by-side ATR-1 irradiation, and specifically how these properties relate to the alloy type, composition, as well as the unirradiated microstructure and properties.

To provide a basis to determine how the current ATR-1 results compare to those previously reported on the same, or similar, alloys; and how might the differences depend on finer details of the specific alloy heat, such as interstitial impurity compositions, as well as the unirradiated microstructures and properties. The latter objective primarily pertains to understanding the 12% Cr TMS and 14% Cr ODS that retain a high uniform strain capacity.

To establish relations between various alloy's strength and ductility unirradiated properties and the corresponding irradiated property changes.

Four out of the five TMS alloys in the unique ATR-1 database behave in a generally expected manner as does the ODS alloy. However the 12Cr TMS, which is a new heat of HT9 steel, experiences a much smaller loss of uniform strain than the lower Cr alloys and previous heats of HT9. An analysis of the s(e) and σ(ε) curves for the five TMS steels shows that the strain hardening rate is highest in the HT9 in both the unirradiated and irradiated conditions, partly rationalizing the correspondingly higher ε_u. However, the reasons for the higher strain-hardening rate in the new HT9 heat are not yet fully understood. Higher strain-hardening rates are broadly related to microstructural features and length scales that mediate dislocation multiplication and annihilation rates; smaller length scales lead to higher hardening rates. However, the new heat of HT9 also has a much lower interstitial free nitrogen (N) content than previous irradiated alloys. Notably, various studies have linked lower free N to higher ductility in Fe-based bcc alloys [26,27].

3. Experimental materials and methods

The irradiation results reported here are from a large, multi-purpose, University of California Santa Barbara-led irradiation program carried out in the Advanced Test Reactor (ATR) at the Idaho National Laboratory (INL), as part of the ATR Nuclear Science Users Facility (NSUF) Program. One of many purposes of the UCSB ATR-1 experiment was to irradiate a large number of candidate structural alloys “side-by-side” at nearly identical temperatures and dpa, so that relatively direct comparisons of changes in their microstructures (not discussed here) and mechanical properties could be made without many of the usual confounding factors encountered in analyzing results from different irradiations. Here we focus on the results of tensile tests on five 9-12Cr TMS and one ODS alloy. The TMS include: HT-9 (H9), T91 (T1), F82H-IAEA (F2), NF616 (N6) and Eurofer97 (E9), where the (X#) notation indicates the compact alloy identification code used here. Note, while the other alloys have been irradiated in previous programs, this study included a new heat of HT9 produced by Metalwerks for the Fuel Cycle Research and Development (FCRD) program following a strict quality assurance program (NQA-1 standards). The measured alloy compositions and the TMS normalized and tempered heat treatments are also summarized in Table 1. This MA957 ODS alloy was processed by ball milling Y_2O_3 and elemental powders, followed by consolidation via hot extrusion at ≈1100 °C [28].

The irradiation was carried out in the A10 position in the ATR over a range of nominal temperatures from ≈290 to 750 °C, and displacement damage doses from ≈1.7 to 6.5 dpa. A large number and wide range of specimen types (1375 in total) were contained in 32 UCSB-designed sub-packets that optimized gas gap temperature control and minimized the corresponding specimen temperature uncertainties in the un-instrumented drop-in ATR A10 position test train. The as-run fluxes and fluences were calculated by the MCNP code, and varied over the 110 cm length of the 10 mm ID capsule, with a mid-core peak of flux ≈2.3×10^{14} n/cm^2-s (E > .1 MeV), corresponding to ≈3.5×10^{-7} dpa/s, and a fluence ≈4×10^{21} n/cm^2. The temperatures were determined by detailed finite element thermal analyses conducted independently by both UCSB and INL. Further details on the UCSB ATR-1 experiment are described elsewhere [29]. The average irradiation conditions for the tensile specimens were ≈296 °C and 6.5 dpa. After irradiation and recovery from the test train in the Hot Fuel Examination Facility (HFEF) at INL, 12 sub-packets were transported in a Type A radioactive shipment to Los Alamos National Laboratory (LANL) for disassembly at the CMR Wing 9 hot cells. Individual specimens were ultrasonically cleaned in a degreaser followed by an acetone wash to remove any possible alpha contamination.

The tensile tests were carried out on sub-size SSJ-2 type specimens with a reduced gage length of 5 mm length, 1.2 mm width and .5 mm thickness. The tensile tests in the LANL CMR hot cells were carried out on an Instron 5567 screw driven test machine at a strain rate of 5×10^{-4}/s at both ≈25 °C and 300 °C. The specimens were shoulder loaded to provide good alignment in tension. The thickness and width of the gage section of all the individual specimens were measured prior to testing. The elevated temperature tensile tests were performed in an inert argon atmosphere. In general, two irradiated tests were carried out at 25 °C, but only one test was conducted at 300 °C. The redundant s(e) curves at 25 °C were very similar in all cases. A minimum of 2 tensile tests, and generally more, were carried out on the unirradiated controls at both 25 °C and 300 °C. The raw digitized load and load point displacement data were converted to nominal engineering stress–strain s(e) curves used in the subsequent derivation of the σ(ε).

4. Analysis of true stress–strain σ(ε) constitutive laws

As noted previously, true stress–strain σ(ε) constitutive laws are needed for quantitative FEM, and other, analysis of the deformation and fracture in arbitrary geometries ranging from test coupons to complex in-service structures, including under both normal operation and transient accident conditions. Developing σ(ε) for irradiated alloys from tensile tests is a challenge if they undergo a plastic instability and necking at very low uniform strains, e_u. Details of the iterative finite element analysis are described elsewhere [14,30], and will be the subject of a future publication that describes details about the derivation of the results shown in Section 5 including and analysis of large geometry changes (LGC) during necking. Briefly, the analysis reported here involves FEM simulation of the s(e) curves based on input trial σ(ε) functions that are systematically modified until the predicted and measured s(e) curves converge. The FEM simulations are carried out using the Abaqus™ package assuming isotropic J_2-flow theory and using piecewise

Table 1
Alloy compositions (wt.%) and heat treatments.

Alloy	C	Cr	Mn	Ni	Si	Mo	Nb	V	W	O	N	P	S	Al	Cu	Co	Ti	Fe
HT-9	.201	12.49	.41	.60	.28	1.07	<.002	.29	.52	.002	.001	.007	<.0005	.015	.034	–	–	Bal
Eurofer97	.117	8.69	.47	.024	.056	.005	<.002	.20	.82	.003	.023	.004	.002	.009	.023	.011	.006	Bal
F82H	.093	7.89	.16	.026	.12	.005	<.002	.16	1.21	.003	.008	.004	.002	.002	.028	.007	.002	Bal
NF616	.108	9.71	.46	.064	.056	.47	.043	.20	1.22	.003	.060	.007	.001	.003	.035	.015	.003	Bal
T91	.052	9.22	.46	.18	.24	.96	.063	.24	.013	.002	.057	.016	.001	.009	.087	.021	.002	Bal
MA957	.02	13.57	.07	.10	.03	.30	<.002	–	–	.22	–	.004	.006	.09	.01	–	.98	Bal +.25 Y2O3

Heat treatments: HT9- 1040°C-1hr./air cool, 760 °C 1hr./air cool; T91- 1040°C-1hr./air cool, 760 °C 1hr./air cool; F82H IAEA- 1040 °C-40 min./air cool, 750 °C 1hr./air cool; Eurofer97- 980 °C-27 min./air cool, 760 °C 90 min./air cool; NF616- Hot Rolled at 1025 °C/air cool; 750°C-2hr./air cool.

segmented input $\sigma(\varepsilon)$ curves. Note the convergence requirement is only up to the strain marking a more rapid drop-off in the measured s(e) curve (load), that is believed to be associated with the development of significant internal micro-void damage. We assume that internal damage and cracking can be ignored at lower strains, although this leads to some uncertainty in the derived $\sigma(\varepsilon)$. Additional measurements of LGC and 3D strain maps, using techniques like digital image correlation, and tests in other geometries (like indentation hardness, bending and compression) can be used to verify further the iterative FE simulations, based on their self-consistency with the test observables [23].

5. Results

Here we use the method described in Section 4 to extract $\sigma(\varepsilon)$ from engineering s(e) curves. Fig. 1 shows the results for both un-irradiated and irradiated conditions on a consistent e-or ε-scale up to 50%. Fig. 1(a–l) summarizes the results of the analysis for the six alloys in this study at 25 °C (1a-f) and 300 °C (1g-l), respectively. Each plot for a specific alloy shows the unirradiated (blue) and irradiated (red) s(e) curves (heavy dashed lines) along with the corresponding derived $\sigma(\varepsilon)$ curves (heavy dotted lines) and the converged FEM prediction of the s(e) curve (light solid line). In this case limited LGC comparisons showed that post-test images of the broken specimens are in good agreement with FE simulations in terms of the neck shapes and dimensions. Note, the diffuse necking behavior is in contrast to a paper in the literature for a A533B steel irradiated at low temperature (<100 °C) that shows failure by a single large shear band that reaches the tensile specimen surfaces [31].

In all cases the unirradiated alloys continuously strain harden, albeit at various rates. However, following irradiation the $\sigma(\varepsilon)$ fall into one of three general classes of behavior: i) strain softening up to $\varepsilon \approx 10–20\%$, followed by an approximately constant, perfectly plastic $\sigma(\varepsilon)$; ii) a very small range of strain hardening followed by a constant perfectly plastic $\sigma(\varepsilon)$; and iii) continuous strain hardening. For tests at 25 °C, type i behavior is observed for F2, E9 and N6, type ii for T1 and type iii for H9 and M7. At 300 °C the pattern is similar, but N6 continues to slowly soften up to 50% and the H9 displays type ii behavior. For tests at 25 °C the F2, E9 and N6 irradiated $\sigma(\varepsilon)_i$ approach the unirradiated $\sigma(\varepsilon)_u$ at $\varepsilon \approx 50\%$, while the $\sigma(\varepsilon)_i$ remains higher for T1, H9 and M7. In the case of the 300 °C tests, the $\sigma(\varepsilon)_i$ remain significantly higher than the $\sigma(\varepsilon)_u$ over the entire strain range examined.

Note that we have previously carried out a similar analysis of F2 tensile test data from High Flux Isotope Reactor irradiations [14,30]. In the dose range of ≈4.9 to 18 dpa at ≈300 °C and for strains up to 50%, one case showed strain softening, while another was closer to perfectly plastic with slight strain hardening following a nearly perfectly plastic low strain increment with slight softening. However, in a third case, significant, continuous strain hardening was observed after a small increment of perfectly plastic flow. And in all three cases at more than 7 dpa, strain hardening was found at even higher strains. Possible effects of high levels of He, produced in a spallation proton irradiation, on $\sigma(\varepsilon)_i$ were also observed. The reasons for the similarities and differences between these previous and current results will be explored in future research.

As noted previously, the plastic strain range between 0 and 10% is especially important since this probably represents a practical structural limit and since this plastic strain range plays a dominant role in both hardness and fracture toughness. Fig. 2a and b compare the $\Delta\sigma_y$ and the average flow stress between 0 and 10% ε ($\Delta\sigma_{10}$) for all the alloys at both 25 and 300 °C, respectively. In general the changes in $\Delta\sigma_{10}$ are less than $\Delta\sigma_y$, with the largest differences for F2, E7 and N6 at 25 °C. On average, $\Delta\sigma_{10} \approx 0.78\Delta\sigma_y$ at both test temperatures.

The corresponding yield stress $s_y \approx \sigma_y$ and s_{uts} are summarized in Table 2 both in terms of the absolute values and the irradiation induced changes. Table 2 also summarizes corresponding ductility data for e_{ui} and e_{ti}. The TMS $\Delta\sigma_y$ vary at 25 °C from ≈540 (H9) to 370 (N6) MPa while the corresponding e_{ui} at 25 °C ranges from 4.0 (H9) to 0.60 (F2) %. As more clearly seen in Fig. 3a the largest $\Delta\sigma_y$ for tests at 25 °C was for H9 followed by T1, E7, N6 and F2. The corresponding $\Delta\sigma_y$ for ODS M7 is much lower than for the TMS alloys. Fig. 3b shows the plot of the $\Delta\sigma_y$ versus Δs_{uts} at 25 °C. The fit line has a slope of ≈.8, which is broadly consistent with the author's previous observations.

Fig. 4 shows that all of the irradiated TMS alloys with ≈9Cr tested at 25 °C have low e_{ui} (<≈ 1%), while the e_{ui} for the 12Cr HT9 alloy is much higher at ≈4.54%. The highest to lowest e_{ui} ranking for the TMS is H9 >> T1 > (slightly) E7 ≈ F2 ≈ N6. The only difference that is statistically significant is the higher e_{ui} for H9. The unirradiated e_{uu} of H9 is also the highest, but it is not nearly as dissimilar to the e_{uu} for the other lower Cr TMS as in the irradiated condition. Likewise the irradiated total elongation is highest in H9, but is similar for the other alloys. Notably, the post-necking $[e_t - e_u]$ ductility is similar in all the TMS averaging ≈ 11.2 ± 2.2%. Thus the effects of irradiation on ductility are mainly to increase hardening and lower strain hardening rates that in combination generally reduce the strains at plastic instability in a tensile test.

Fig. 5a shows that the $\Delta\sigma_y$ for 25 °C tests tracks those at 300 °C with a slope of ≈.9, which is consistent with previous experience and the ratio of the corresponding shear moduli. As shown in Fig. 5b, there is not a fully consistent pattern in the irradiated e_{ui} at 25 versus 300 °C. In 4 of the 6 cases the e_{ui} at 300 °C are lower and in 2 cases they are higher than at 25 °C. An overall fit to e_{ui}(300 °C) versus e_{ui}(25 °C) gives a higher temperature intercept of .66 and a slope of .62, suggesting that on average the tensile ductility decreases over this temperature interval, as is the case for the unirradiated condition. However, as seen in Fig. 5b, perhaps with the exception of Eurofer97, the overall alloy-to-alloy pattern of irradiated e_{ui} is similar at both test temperatures.

We have also examined the inter-relationships between various tensile properties that will be detailed in future publications for a

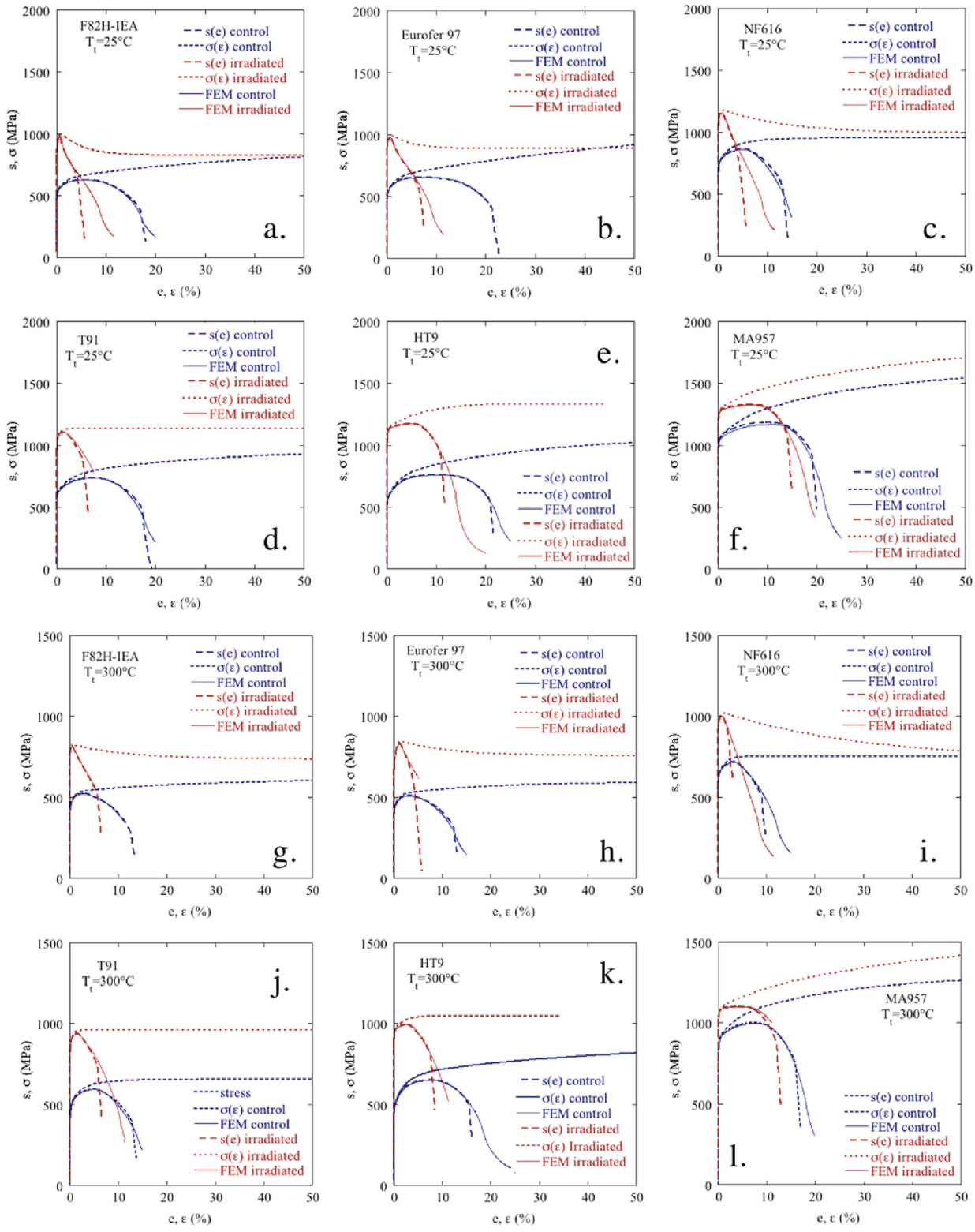

Fig. 1. The s(e) curves at 25 and 300 °C that were used to derive the corresponding σ(ε) constitutive curves using the FEM procedure for the 6 alloys in the unirradiated and irradiated conditions (see text).

larger matrix of alloys that includes one austenitic stainless steel and several additional ODS alloys. However, as a preview, Fig. 6 shows the variation of the $\Delta\sigma_{yi}$ and $\Delta\sigma_{ui}$ for tests at 25 °C, with the corresponding unirradiated σ_y for 11 alloys irradiated in ATR-1. While there is some scatter, the decrease in irradiation hardening, $\Delta\sigma_y$, with increasing unirradiated alloy σ_{yu} is clear and compelling. There are several explanations for this trend, such as strengthening superposition rules [32], but further analysis is beyond the scope of this paper.

The tensile data trends summarized above are generally consistent with previous observations, but provide a degree of quantification that has not been previously reported, as well as some new insights. The exception to these general trends is the

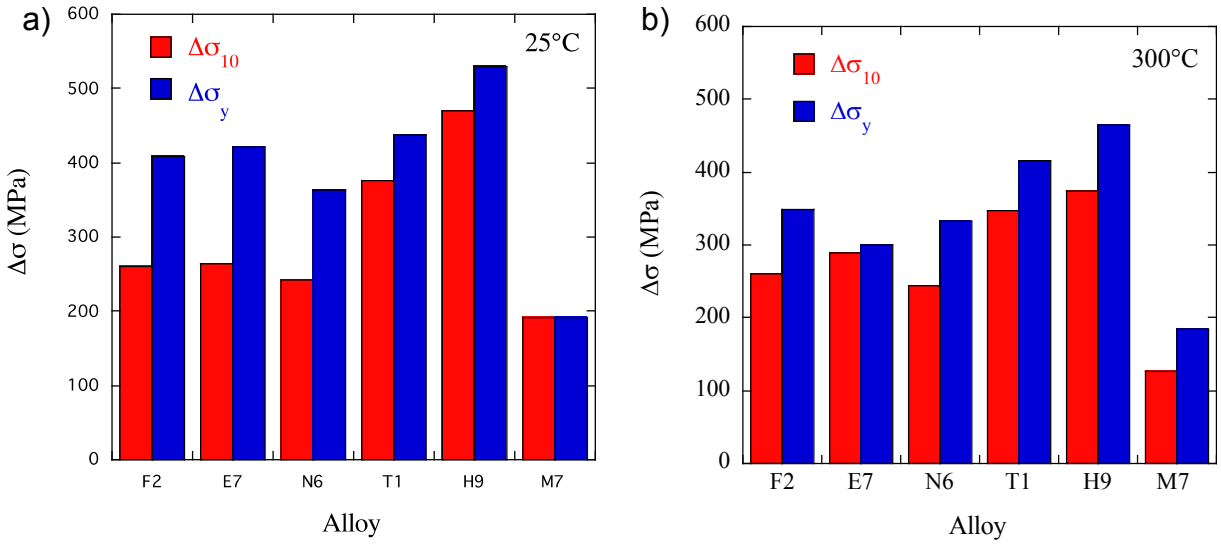

Fig. 2. Changes in the average flow stress between 0 and 10% strain ($\Delta\sigma_{10}$) and the corresponding $\Delta\sigma_y$ for tests at: a) 25 °C; b) 300 °C.

Table 2
Summary of the engineering tensile data.

Alloy	σ_{yu}	s_{uu}	$\Delta\sigma_y$	Δs_u	e_{uu}	e_{tu}	e_{ui}	e_{ti}
H9	555/465	757/652	535/480	406/304	9.4/8.4	21.2/15.6	4.0/2.5	19.33/7.6
T1	610/453	730/596	420/427	360/343	6.8/4.8	16.9/12.9	1.0/1.5	4.7/5.8
N6	735/630	860/719	375/330	284/284	5.4/3.3	13.7/9.1	.60/.68	4.3/2.7
F2	521/450	627/522	367/352	330/297	5.3/2.8	17.3/12.7	.60/.51	5.3/5.9
E7	528/425	651/510	397/300	313/322	6.9/3.0	20.3/12.5	.70/2.2	6.3/4.2
M7	1033/890	1178/1002	213/180	134/102	9.9/6.0	19.9/16.0	6.1/3.6	14/12.0

The xxx/yyy format indicates data at 25/300 °C. Units: stress (MPa), strain (%).

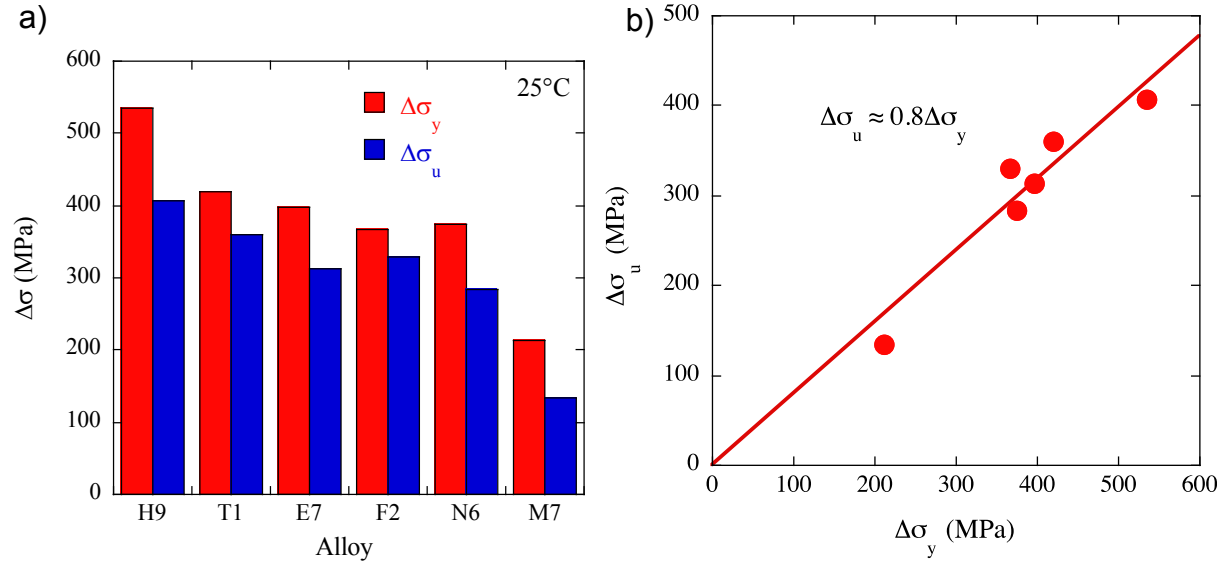

Fig. 3. a) $\Delta\sigma_y$ and $\Delta\sigma_u$ for tests at 25 °C; b) a plot of the corresponding $\Delta\sigma_y$ versus $\Delta\sigma_u$.

higher irradiated e_u of HT9. Previous studies reported lower e_u (<1%) in other heats of H9 for irradiations at temperatures less than 350 °C to similar dpa [3]. Possible reasons for the behavior of H9 are discussed in the following section.

6. Discussion of the higher ductility of irradiated MA-957 and HT-9

The higher ductility of the MA957 is relatively easy to understand and is largely related to the fine grain size on the order of 1 μm or less. The fine grains result in higher strain hardening rates due to the higher generation rate of dislocations. Limited slip length leads to a

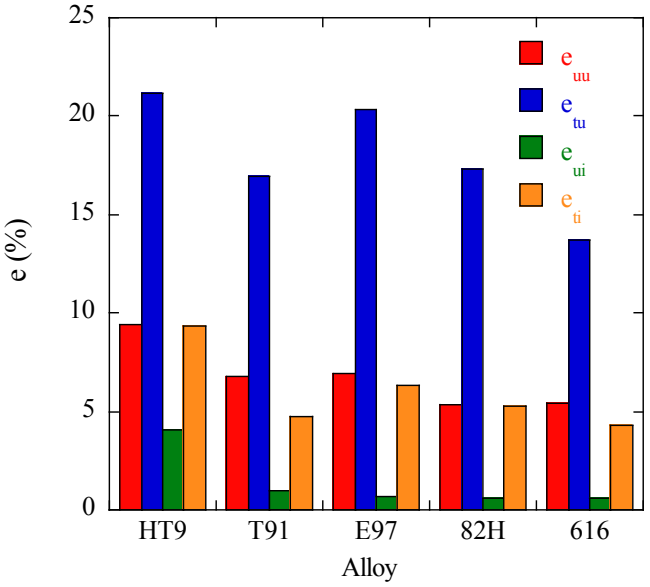

Fig. 4. Comparison of the unirradiated and irradiated e_u and e_i for the 5 TMS alloys.

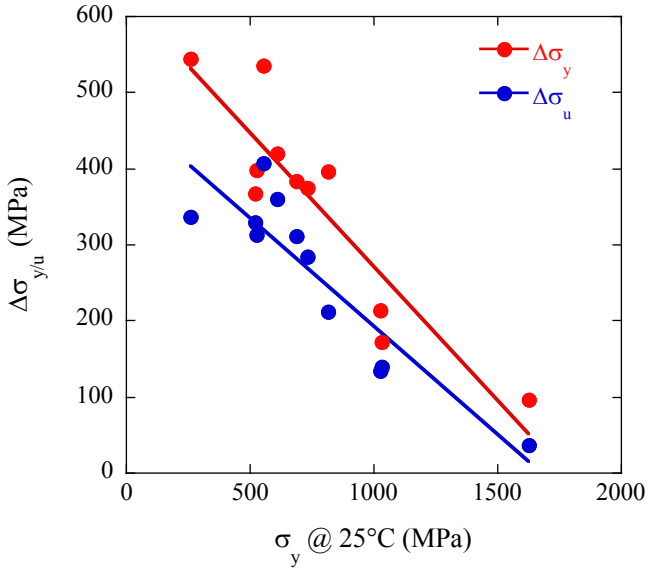

Fig. 6. The $\Delta\sigma_y$ and $\Delta\sigma_u$ versus the unirradiated σ_y for tests at 25 °C.

high concentration of forest sources and generation of geometrically necessary dislocations which also scale with the inverse of the grain size. Further more, MA957 contains subgrain and matrix features that can enhance dislocation multiplication like strong precipitates that act as bowing sources. Additionally, the fine grains limit the length and propagation of nascent localized shear bands.

There may be similar microstructurally-based contributions to the higher strain hardening and uniform strain ductility in the new heat of HT-9. The increase in yield stress after irradiation and reduced loss of ductility may be from different defect–dislocation interactions, which may explain why hardening was observed similar to previous irradiations while uniform elongation was retained. Unfortunately, the unirradiated and irradiated microstructures of this alloy remain to be characterized. This will be explored in future work, which will include studies of the deformed microstructures as well.

There is another possible contributing factor. As noted above, low temperature ductility in ferritic/martensitic steels is affected by localized flow. Previous research has shown that localized flow in ferritic alloys is very sensitive to the free carbon (C) and nitrogen (N) content. For example, C and N content are widely known to affect Luder's band formation [33,34]. In research by Liu et al. [33], a high purity Fe-17Cr ferritic steel alloyed with Nb was tested after slow and rapid cooling heat treatments. Slow cooling allows the Nb to form carbides and nitrides, thus removing C and N interstitials from solution. Yield drops and Luder's bands were observed in the rapidly cooled condition, while smooth and uniform yielding was observed in the slow cooled condition. Further, it has been long known that the mechanical properties (e.g. impact strength and toughness) of Fe–Cr alloys are also strongly affected by C and N in

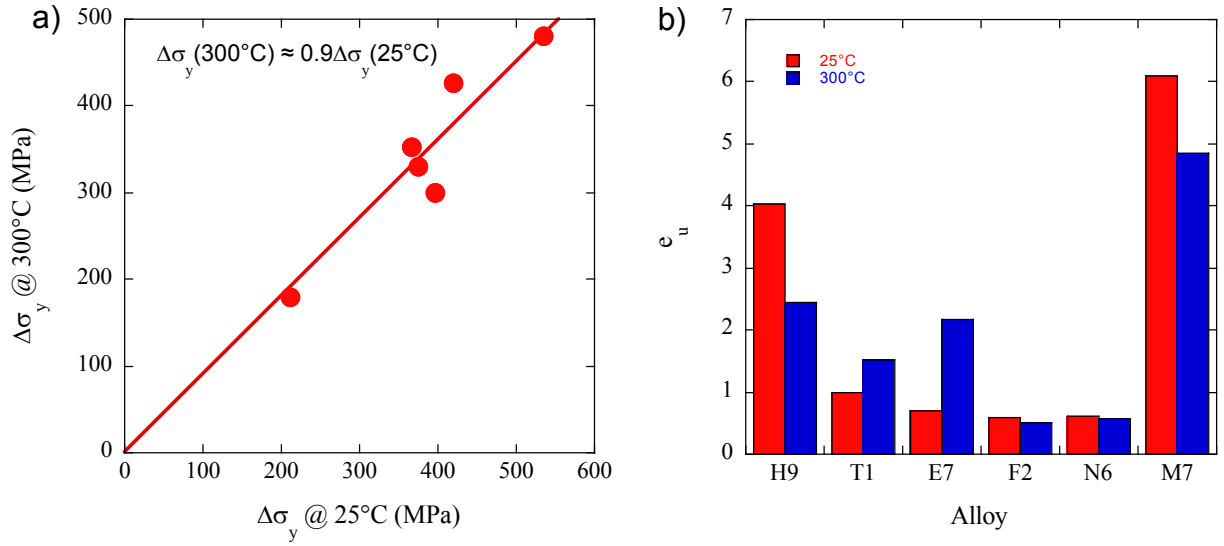

Fig. 5. a) $\Delta\sigma_y$ for tests at 300 °C versus 25 °C; b) e_{ui} at 25 and 300 °C.

solution [27,35]. More recently, interstitial-free ferritic steels have been developed, in large part because of their improved resistance to localized flow. Examples include super-ferritic alloys such as S44627, S44635, and S44660 where Ti and Nb are added, again to remove N and C from solution. For example, a review by Hoile [36] shows how the R-ratio failure limit (plastic strain ratio of width to thickness directions in a sheet) [37] is improved with additions of Ti or Nb in nearly interstitial free steels. Note that tensile test results in Fig. 1 show that T1 has the second best uniform elongation after irradiation and this alloy contains the highest amount of Nb (.63 wt %). In addition to previous research, more recent papers have noted the effects of light elements in Fe such as C effects on dislocation loop evolution [38] and segregation of C at dislocation loops [39]. These observations are examples that demonstrate that free C and N could significantly affect mechanical properties in ferritic steels at low temperatures. Notably, these effects may be preserved in the irradiated condition, and indeed may be further enhanced if large populations of defects, like dislocation loops, trap additional free C and N interstitial solutes.

7. Summary and conclusions

Tensile test results at 25 and 300 °C on five 9-12Cr tempered martensitic steels and one 14Cr oxide dispersion strengthened alloy, that were side-by-side irradiated to 6.5 dpa at 295 °C in the Advanced Test Reactor (ATR), are reported. The main results and conclusions include:

- The irradiated $\sigma(\varepsilon)$ laws for these alloys, derived from engineering stress-strain curves, fall into categories of: strain softening, nearly perfectly plastic, and strain hardening.
- Significant variations in $\Delta\sigma_y$ and reductions e_{ui} are observed, where the e_{ui} trends can be understood in terms of the alloy's $\sigma(\varepsilon)$ behavior.
- Differences in the average $\sigma(\varepsilon)$ increases in the range of 0–10% strain are smaller than the corresponding $\Delta\sigma_y$, and vary more from alloy to alloy. This has important implications to irradiated properties like fracture toughness.
- The observed relation of $\Delta\sigma_{10} \approx 0.8\Delta\sigma_y$ is consistent with previous observations.
- The observed relation of $\Delta\sigma_y(300\ ^\circ C) \approx 0.9\Delta\sigma_y(25\ ^\circ C)$ is consistent with previous observations.
- The observed decrease in $\Delta\sigma_u$ and $\Delta\sigma_y$ with increases in σ_{yu} is not unexpected, but has not been fully analyzed.
- In five out of six cases the effects of irradiation are generally consistent with previous observations. However, the particular heat of the 12Cr HT-9 tempered martensitic steel in this study has a much higher e_u than observed for earlier heats. The reasons for this behavior are not understood and may be microstructural in origin.
- However, it is noted that the new heat of HT-9, procured under modern quality assurance standards, has lower interstitial free N than previous heats. Notably, there is a general relation between lower interstitial solute contents and improved ductility, and homogenous deformation, in broadly similar steels.

Acknowledgments

This work at LANL was funded under the Advanced Fuels Campaign of the Department of Energy's (DOE) Fuel Cycle Research and Development Program. The work at UCSB was funded by DOE NEUP (NU-11-3150) and Office of Fusion Energy Science (DE-FG03-94ER54275) grants. The UCSB ATR-1 irradiations were carried out as part of the National Scientific Users Facility program, with the assistance of a large number of outstanding engineers. The help of Colin Knight in arranging shipment of the specimens from INL to LANL is greatly appreciated. Special thanks also go to UCSB staff members Doug Klingensmith and David Gragg who played the key roles in building the experiment and former PhD student, Dr. Nicholas Cunningham, who carried out the thermal design analysis.

References

[1] S.A. Maloy, M. Toloczko, J. Cole, T.S. Byun, J. Nucl. Mater. 415 (2011) 302–305.
[2] J.L. Straalsund, R.W. Powell, B.A. Chin, J. Nucl. Mater. 108–109 (1982) 299–305.
[3] O. Anderoglu, T.S. Byun, M. Toloczko, S.A. Maloy, Metall. Mater. Trans. A Phys. Metall. Mater. Sci. 44A (2013) S70–S83.
[4] G.R. Odette, J. Nucl. Mater. 155 (1988) 921–927.
[5] G.R. Odette, M.J. Alinger, B.D. Wirth, Recent Developments in Irradiation-Resistant Steels, Annual Review of Materials Research, Annual Reviews, Palo Alto, 2008, pp. 471–503.
[6] Y. Dai, G.R. Odette, T. Yamamoto, The effects of helium in irradiated structural alloys, in: Elsevier (Ed.), Comprehensive Nuclear Materials, vol. 1, 2012.
[7] M.B. Toloczko, F.A. Garner, C.R. Eiholzer, J. Nucl. Mater. 212 (1994) 604–607.
[8] T. Yamamoto, Y. Wu, G.R. Odette, K. Yabuuchi, S. Kondo, A. Kimura, J. Nucl. Mater. 449 (2014) 190–199.
[9] G.R. Odette, P. Miao, D.J. Edwards, T. Yamamoto, R.J. Kurtz, H. Tanigawa, J. Nucl. Mater. 417 (2011) 1001–1004.
[10] T. Yamamoto, G.R. Odette, H. Kishimoto, J.W. Rensman, P. Miao, J. Nucl. Mater. 356 (2006) 27–49.
[11] J. Henry, X. Averty, A. Alamo, J. Nucl. Mater. 417 (2011) 99–103.
[12] B. van der Schaaf, C. Petersen, Y. De Carlan, J.W. Rensman, E. Gaganidze, X. Averty, J. Nucl. Mater. 386–88 (2009) 236–240.
[13] R.J. Kurtz, A. Alamo, E. Lucon, Q. Huang, S. Jitsukawa, A. Kimura, R.L. Klueh, G.R. Odette, C. Petersen, M.A. Sokolov, P. Spätig, J.W. Rensman, J. Nucl. Mater. 386–88 (2009) 411–417.
[14] T. Yamamoto, G.R. Odette, M.A. Sokolov, J. Nucl. Mater. 417 (2011) 115–119.
[15] G.R. Odette, T. Yamamoto, H.J. Rathbun, M.Y. He, M.L. Hribernik, J.W. Rensman, J. Nucl. Mater. 323 (2003) 313–340.
[16] G.R. Odette, H.J. Rathbun, M. Hribernik, T. Yamamoto, M. He, P. Spatig, Materials issues for generation IV systems: status, open questions and challenges, in: Proceedings of the NATO ASI Science for Peace and Security Series B: Physics and Biophysics, Springer, 2008, p. 203.
[17] G.R. Odette, M.Y. He, T. Yamamoto, J. Nucl. Mater. 367 (2007) 561–567.
[18] G.R. Odette, M.Y. He, J. Nucl. Mater. 307 (2002) 1624–1628.
[19] H.J. Rathbun, G.R. Odette, T. Yamamoto, G.E. Lucas, Eng. Fract. Mech. 73 (2006) 134–158.
[20] H.J. Rathbun, G.R. Odette, M.Y. He, T. Yamamoto, Eng. Fract. Mech. 73 (2006) 2723–2747.
[21] T.S. Byun, N. Hashimoto, K. Farrell, E.H. Lee, J. Nucl. Mater. 349 (2006) 251–264.
[22] M. Victoria, N. Baluc, C. Bailat, Y. Dai, M.I. Luppo, R. Schaublin, B.N. Singh, J. Nucl. Mater. 276 (2000) 114–122.
[23] G.R. Odette, M.Y. He, E.G. Donahue, P. Spatig, T. Yamamoto, J. Nucl. Mater. 307 (2002) 171–178.
[24] G.R. Odette, D.T. Hoelzer, JOM 62 (9) (2010) 84–92.
[25] G.R. Odette, JOM 66 (2014) 2427–2441.
[26] K.L. Murty, J. Metals 37 (1985) 34–39.
[27] A. Hishinuma, S. Takaki, K. Abiko, Phys. Stat. Sol.(a) 189 (2002) 69–78.
[28] N. Cunningham, Y. Wu, D. Klingensmith, G.R. Odette, Mater. Sci. Eng. A Struct. Mater. Prop. Microstruct. Process. 613 (2014) 296–305.
[29] G.R. Odette, T. Yamamoto, B. Sams, D. Klingensmith, N. Cunningham, G. Waches, J.I. Cole, P.E. Murrey, Summary of the USCB Advanced Test Reactor National Scientific Users Facility Irradiation Experiment, DOE/ER-0313/46, 2009, p. 79.
[30] T. Yamamoto, G.R. Odette, Y. Wu, Fusion Materials Semi-Annual Report 7/1/2011 to 12/31/2011, DOE/ER-0311/51, 2012, pp. 78–84.
[31] J.W. Kim, T.S. Byun, Nucl. Eng. Technol. 44 (2012) 953–960.
[32] G.R. Odette, G.E. Lucas, Radiat. Eff. Defects Solids 144 (1998) 189–231.
[33] Z.Y. Liu, F. Gao, L.Z. Jiang, G.D. Wang, Mater. Sci. Eng. A Struct. Mater. Prop. Microstruct. Process. 527 (2010) 3800–3806.
[34] F. Gao, W. Zhang, Z. Zhang, Z. Liu, G. Wang, Precipitates and luders elongation in ferritic stainless steels stabilized with Ti and V, Pts 1-3, in: J.M. Zeng, T.S. Li, S.J. Ma, Z.Y. Jiang, D.G. Yang (Eds.), Advanced Engineering Materials, 2011, pp. 16–19.
[35] W.O. Binder, H.R. Spendelow Jr., Trans. ASM 43 (1951) 759–777.
[36] S. Hoile, Mater. Sci. Technol. 16 (2000) 1079–1093.
[37] M. Grumbach, G. Pomey, Sheet Met. Ind. 43 (1966) 515–529.
[38] D. Terentyev, I. Martin-Bragado, Scr. Mater. 97 (2015) 5–8.
[39] D. Terentyev, A. Bakaev, E.E. Zhurkin, J. Phys. Condens. Matter. 26 (2014) 165402.